Int. J. Multiphase Flow Vol. 18, No. 6, pp. 927–941, 1992
Printed in Great Britain

0301-9322/92 $5.00 + 0.00
Pergamon Press Ltd

DIRECT NUMERICAL SIMULATION OF PARTICLE BEHAVIOUR IN THE WALL REGION OF TURBULENT FLOWS IN HORIZONTAL CHANNELS

S. PEDINOTTI,[1] G. MARIOTTI[1] and S. BANERJEE[2]

[1]ENEL—Thermal and Nuclear Research Center, Via Andrea Pisano 120, 56122 Pisa, Italy

[2]Department of Chemical & Nuclear Engineering, University of California Santa Barbara, CA 93106, U.S.A.

(Received 15 September 1991; in revised form 5 August 1992)

Abstract—The motion of small particles in the wall region of turbulent channel flows has been investigated using direct numerical simulation. It is assumed that the particle concentration is low enough to allow the use of one-way coupling in the calculations, i.e. the fluid moves the particles but there is no feedback from the particles on the fluid motion. The velocity of the fluid is calculated by using a pseudospectral, direct solution of the Navier–Stokes equations. The calculations indicate that particles tend to segregate into the low-speed regions of the fluid motion near the wall. The segregation tendency depends on the time constant of the particle made non-dimensional with the wall shear velocity and kinematic viscosity. For very small and very large time constants, the particles are distributed more uniformly. For intermediate time constants (of the order 3), the segregation into the low-speed fluid regions is the highest. The finding that segregation occurs for a range of particle time constants is supported by experimental results. The findings regarding the more uniform distributions, however, still remain to be verified against experimental data which is not yet available. For horizontal channel flows, it is also found that particles are resuspended by ejections (of portions of the low-speed streaks) from the wall and are, therefore, primarily associated with low-speed fluid. The smaller particles are flung further upwards and, as they fall back towards the wall, they tend to be accelerated close to the fluid velocity. The larger particles have greater inertia and, consequently, accelerate to lower velocities giving higher relative velocities. This velocity difference, as a function of wall-normal distance, follows the same trend as in experiments but is always somewhat smaller in the calculations. This appears to be due to the Reynolds number for the numerical simulation being smaller than that in the experiment. It is concluded that the average particle velocity depends not only on the wall variables for scaling, but also on outer variables associated with the mean fluid velocity and fluid depth in the channel. This is because fluid depth in combination with the wall shear velocity determines how much time a particle, of a given size and density, spends in the outer flow and, hence, how close it gets to the local fluid velocity.

Key Words: particles, deposition, turbulence

1. INTRODUCTION

The motion of particles in turbulent flows has become one of the most interesting topics in fluid mechanics because of the richness of fundamentally interesting phenomena that arise, and the many practical applications. For example, the deposition of particles in aerosols is important in many environmental problems. Similarly, particle behaviour near solid walls is fundamental to an understanding of fouling, the design of electrostatic precipitators and many other energy conversion/pollution control devices. In view of this, a number of experimental and computational studies have been conducted, most recently in plane mixing layers, by Kobayashi *et al.* (1988), Kamulu *et al.* (1989) and Lazaro & Lasheras (1989). Computational studies on how turbulence structure affects the particle distribution have also been investigated by Maxey (1987), using Fourier modes and the particles as a compressible flow field, and by Chein & Chung (1987) for mixing layers using vortex methods. Squires & Eaton (1990) have used direct simulation of homogeneous isotropic turbulence to study particle segregation phenomena.

In all these studies there is evidence that denser-than-fluid particles tend to get flung out of regions of high vorticity and into regions of low vorticity and high strain rate. This preferential accumulation of particles can, in turn, modify the turbulence characteristics of the continuous fluid, as shown in the recent experimental study by Rashidi *et al.* (1990). Rashidi *et al.* (1990), performed experiments in water channel flow, using a range of particle size with non-dimensional diameters varying from about 10 to 1, where the non-dimensionalization was done with the wall shear velocity

and kinematic viscosity. Even at relatively low particle volume fractions, of the order 10^{-4} volume percent, they found significant effects on the turbulence intensities when the particle diameters were in the larger range. They also showed that these larger particles tended to segregate into the low-speed fluid regions, i.e. the so-called low-speed streaks that are the primary organized fluid structures very close to the wall. However, Rashidi *et al.* (1990) did not measure the particle distributions for the smaller sizes and found that while the smaller particles did, on average, lag the local fluid velocity throughout the channel, the lag was smaller than that for the particles in the larger size range. They did not offer an explanation why this occurred and why the smaller particles had only marginal effects on the turbulence intensities.

Turning now to calculations of particle motion in wall turbulent flows, the only other direct simulation of which we are aware has been by McLaughlin (1989). McLaughlin was primarily interested in the deposition of aerosol particles with densities much greater than that of the fluid. He reports a relatively coarse pseudospectral solution of the Navier–Stokes equations with the assumption that the fluid velocity is unaffected by the presence of particles, i.e. "one-way coupling", in that particles are moved by the fluid but no reaction force is incorporated in the fluid motion equations. McLaughlin (1989) was primarily interested in the deposition behaviour of the particles and did not examine whether they segregated in the wall region or the mechanisms for resuspension.

The present study is motivated by these recent experiments and has the primary objective of determining how particles distribute in the wall region. To this end, pseudospectral calculations based on a computer code developed by Lam & Banerjee (1988; Lam 1989; Lam & Banerjee 1992) has been used to generate the fluid velocity field in a horizontal channel. The boundary conditions on the bottom wall are no-slip and the boundary conditions at the channel surface are free-slip. This latter condition corresponds to a free water surface with high surface tension and with interfacial waves of negligible amplitude that essentially reproduces the Rashidi *et al.* (1990) experiments.

Because of limitations in computer memory, the computations were done at a relatively low shear Reynolds number (106), based on the wall shear velocity, half liquid-depth and kinematic viscosity. Lam & Banerjee (1988, 1992) have shown that 32 streamwise modes, 64 spanwise modes and 65 wall-normal modes, using a Fourier–Chebyshev expansion for the velocity field, give sufficient resolution to reproduce the main features of wall turbulent flows at this Reynolds number. They were able to capture the usual (experimental) non-dimensional streak spacing of about 100, ejection and burst frequencies of the right periods and various other turbulence statistics related to moments of the velocity field and correlation functions. This Reynolds number is somewhat lower than the value of 147 for which Rashidi *et al.* (1990) reported most of the experimental data. In view of this, the numerical calculations for particle behaviour cannot be directly compared with the Rashidi *et al.* data, since scaling is not straightforward (as is discussed later). However, most of the qualitative features can be examined and certain predictions can be derived from the numerical calculations which can be checked in future experiments.

In addition to the factors governing particle segregation, we will also discuss mechanisms for particle suspension and reentry into the wall region. In a subsequent paper, there will be detailed discussion of the Lagrangian correlation functions, diffusivities and particle–fluid response functions based on ensemble averaging of the direct numerical simulations. Such averaged quantities, while useful in multiphase turbulence modelling, are of limited interest in understanding the mechanisms responsible for particle motion in the wall region and would, therefore, not contribute directly to the main thrust of the present paper.

2. THEORETICAL ASPECTS AND SCALING

The fluid field is obtained from a direct numerical simulation of horizontal turbulent channel water flow, where the free surface is treated as a slip wall, i.e. no interfacial waves are considered. The numerical method has been discussed in detail elsewhere (Lam & Banerjee 1988; Lam 1989; Lam & Banerjee 1992) and will only be sketched briefly here. The method is essentially the same as that of Kim *et al.* (1987), though the computer code was developed independently.

While the technique is now fairly standard in the direct simulation community, it seems relatively unknown outside this small group. For this reason we include a brief description here.

To summarize, the direct simulation solves the equations for an incompressible, Newtonian fluid, viz.

$$\frac{\partial u_j}{\partial x_j} = 0 \qquad [1]$$

and

$$\frac{\partial u_i}{\partial t} = S_i + \frac{1}{\mathrm{Re}} \nabla^2 u_i - \frac{\partial p}{\partial x_i}, \qquad [2]$$

where

$$S_i = u_j \frac{\partial u_i}{\partial x_j} - \frac{\partial \bar{p}}{\partial x_i}. \qquad [3]$$

Here u_i are the non-dimensional velocity components, $\partial \bar{p}/\partial x_i$ is the mean pressure gradient and $\partial p/\partial x_i$ is the pressure gradient minus the mean part (Note p is the kinematic pressure, i.e. pressure divided by fluid density). All variables are non-dimensionalized with the half-fluid depth h, and the wall shear velocity u^*. The shear Reynolds number is then $\mathrm{Re} = u^* h/\nu$, where ν is the kinematic viscosity.

The boundary conditions are then

$$u_i = 0 \qquad \text{at } x_3 = +1 \qquad [4]$$

at the bottom wall, and

$$\frac{\partial u_1}{\partial x_3} = \frac{\partial u_2}{\partial x_3} = u_3 = 0 \quad \text{at } x_3 = -1 \qquad [5]$$

at the free surface (treated as a slip wall). Note that $x_3 = 0$ at half the channel depth, x_1 is streamwise, x_2 is spanwise and x_3 is wall-normal.

To solve [1] and [2] subject to [4] and [5], it is easier to eliminate the pressure gradient by taking the curl of [2] and using [1] to give

$$\frac{\partial \omega_k}{\partial t} = \varepsilon_{ijk} \frac{\partial S_j}{\partial x_i} + \frac{1}{\mathrm{Re}} \nabla^2 \omega_k, \qquad [6]$$

where $\omega_k = \varepsilon_{ijk}\, \partial u_j/\partial x_i$ is the vorticity and ε_{ijk} is the alternating unit tensor.

Taking the curl of [6] again and using the vector identity $\mathrm{curl}(\mathrm{curl}\,\mathbf{u}) = \mathrm{grad}(\mathrm{div}\,\mathbf{u}) - \nabla^2\mathbf{u}$, we have

$$\frac{\partial}{\partial t}(\nabla^2 u_i) = \nabla^2 S_i - \frac{\partial}{\partial x_i}\left(\frac{\partial S_j}{\partial x_j}\right) + \frac{1}{\mathrm{Re}} \nabla^4 u_i. \qquad [7]$$

For the problem considered here, we solve at first for u_3 and ω_3, i.e.

$$\frac{\partial \omega_3}{\partial t} = \frac{\partial S_2}{\partial x_1} - \frac{\partial S_1}{\partial x_2} + \frac{1}{\mathrm{Re}} \nabla^2 \omega_3 \qquad [8]$$

and

$$\frac{\partial}{\partial t}(\nabla^2 u_3) = \nabla^2 S_3 - \frac{\partial}{\partial x_3}\left(\frac{\partial S_j}{\partial x_j}\right) + \frac{1}{\mathrm{Re}} \nabla^4 u_3. \qquad [9]$$

From this the other velocity components may be obtained by solving simultaneously

$$\frac{\partial u_1}{\partial x_1} + \frac{\partial u_2}{\partial x_2} = -\frac{\partial u_3}{\partial x_3} \qquad [10]$$

and

$$\frac{\partial u_2}{\partial x_1} - \frac{\partial u_1}{\partial x_2} = \omega_3. \qquad [11]$$

The pressure field is not needed in the calculation but can be obtained whenever necessary by solving

$$\nabla^2 p = \frac{\partial S_j}{\partial x_j}. \qquad [12]$$

The S_j are, of course, determined in the main calculations.

The main equations [8] and [9] are advanced in time using a two-level explicit Adam–Bashforth scheme for the convective terms and an implicit Crank–Nicholson method for the diffusive terms. The solutions in the homogeneous directions, i.e. x_1 and x_2, are represented by Fourier expansions with N_1 and N_2 terms, respectively. In the wall-normal direction, N_3 Chebyshev polynomials are used. The technique depends on the non-linear terms, i.e. the S_i terms, being evaluated in physical space as the convolution integrals in wavenumber space would be very time consuming. As such, the basis functions for the velocity field expansion (Fourier and Chebyshev polynomials) are chosen so that the fast Fourier transform algorithm can be used to go back and forth between physical and wavenumber space. This makes the calculations much more efficient, e.g. only 1.5 s CPU time is taken per time step for a $65 \times 64 \times 32$ problem using a CRAY-XMP.

Because of the non-linear terms being explicitly evaluated in physical space (rather than by convolution integrals) the technique is "pseudospectral". The only difficulty arises from the fourth-order equation derived from [9]. This is split into two second-order equations with a rather delicate treatment of the boundary conditions—for details reference should be made to Lam (1989). The ultimate problem then boils down to the solution of a set of second-order Helmholtz-type ordinary differential equations in the x_3 (wall-normal) direction. These are solved by the Chebyshev-tau method (Lanczos 1956; Gottleib & Orszag 1977) for each wavenumber pair (k_1, k_2). Removal of aliasing errors is accomplished by the truncation rule (Schnack *et al.* 1984; Canuto *et al.* 1988).

The velocities at an arbitrary point may be found by evaluating the triple sum using the Chebyshev coefficients denoted here by $\hat{a}_i$:

$$u_i(x_1, x_2, x_3) = \sum^{N_1}\sum^{N_2}\sum^{N_3} \hat{a}_i(k_1, k_2, N_3) \cdot \exp(k_1 x_1 + k_2 x_2) \cdot T_{N_3}(x_3), \qquad [13]$$

where $\hat{a}_i$ are the Chebyshev coefficients, $T_{N_3}(x_3) = \cos(n_3 \cos^{-1} x_3)$ is the Chebyshev polynomial of order N_3. The prime on the first sum denotes that by convention the first term is halved. This is a very time-consuming procedure and it is much faster to obtain velocities, their derivatives etc. at the collocation points using plane-by-plane FFT calculations.

Suffice to say at this point that, for $\mathrm{Re} = 106$, $38 \times 64 \times 65$ modes in the x_1, x_2 and x_3 directions are enough to reproduce all the experimental features of turbulence so far as we are aware, including streak spacing, ejection phenomena and higher-order statistics.

The particles are moved using the following equation (where all quantities are dimensional):

$$\rho_p v_p = -\frac{3}{4}\frac{v_p \rho_f}{d} c_D(\mathbf{v} - \mathbf{u})|\mathbf{v} - \mathbf{u}| + v_p(\rho_p - \rho_f)\mathbf{g} + \text{ other terms} \qquad [14]$$

The other terms, including forces due to "added" mass, hydrostatic, Basset and lift forces, were not considered in most of the calculations. The effect of added mass, hydrostatic and lift forces were in fact checked to be negligible, while the Basset term was not calculated. In [14], v_p refers to the particle volume, ρ_p to its density, $\mathbf{v}$ to its velocity and d to its diameter. The fluid velocity is $\mathbf{u}$ and the fluid density is ρ_f. The drag coefficient is c_D and $\mathbf{g}$ is the gravitational acceleration.

Ignore for the moment the other terms and the consider particle Reynolds number to be low, i.e.

$$\mathrm{Re}_p = \frac{|\mathbf{v} - \mathbf{u}|}{v} < 1,$$

then the Stokes drag law gives

$$c_D = \frac{24}{\mathrm{Re}_p} \qquad [15]$$

and we may write [14] as

$$\frac{\mathrm{d}\mathbf{v}}{\mathrm{d}t} = -\frac{(\mathbf{v}-\mathbf{u})}{\tau_\mathrm{p}} + \frac{\rho_\mathrm{p}+\rho_\mathrm{f}}{\rho_\mathrm{p}}\mathbf{g}, \qquad [16]$$

where

$$\tau_\mathrm{p} = \frac{\rho_\mathrm{p}}{\rho_\mathrm{f}}\frac{d^2}{18\nu} \qquad [17]$$

is a particle time constant.

There are now several possibilities for scaling. Very close to the wall where viscous effects are important, inner scaling is appropriate, i.e. using u^* and ν as the non-dimensionalizing scales. For clarity we define the non-dimensional variables in this case with the superscript "+". The particle motion equation [16] then becomes

$$\frac{\mathrm{d}\mathbf{v}^+}{\mathrm{d}t^+} = -\frac{\mathbf{v}^+ - \mathbf{u}^+}{\tau_\mathrm{p}^+} + \mathbf{g}^+, \qquad [18]$$

where

$$\mathbf{v}^+ = \mathbf{v}/u^*; \quad \mathbf{u}^+ = \mathbf{u}/u^*; \quad t^+ = \frac{tu^{*2}}{\nu}; \quad \tau_\mathrm{p}^+ = \frac{\rho_\mathrm{p}}{\rho_\mathrm{f}}\frac{d^{+2}}{18}; \quad d^+ = \frac{du^*}{\nu}; \quad \mathbf{g}^+ = \frac{(\rho_\mathrm{p}-\rho_\mathrm{f})\nu}{\rho_\mathrm{p}u^{*3}}\mathbf{g}.$$

From [18] it is immediately seen that identical particle motion will be obtained very close to the wall in a given fluid velocity field if τ_p^+ and $\mathbf{g}^+$ are kept the same. Moreover, $\mathbf{u}$ has statistical features that are quite independent of the Reynolds number. For example, the spanwise spacing between low-speed streaks in the wall region is about 100 non-dimensional distance units. Similarly, the time between bursts is about 85 non-dimensional time units (see Rashidi *et al.* 1990).

For these reasons statistical aspects of particle behaviour near the wall may also be scaled, as predicted by [18], at different Reynolds numbers by keeping τ_p^+ and $\mathbf{g}^+$ the same.

In particular, consider experiments done at $\mathrm{Re} = u^*h/\nu = 147$ but calculations possible only at $\mathrm{Re} = 106$, which is the situation here. One would expect from [18] that the behaviour very near the wall would be the same if, as one of several possibilities, the numerical calculations used the same values of h, in the experiments, but

$$u^*(\mathrm{num}) = \frac{106}{147}u^*(\mathrm{exp}),$$

$$d(\mathrm{num}) = \frac{147}{106}d(\mathrm{exp})$$

and

$$\mathbf{g}(\mathrm{num}) = \left(\frac{106}{147}\right)^3\mathbf{g}(\mathrm{exp}).$$

This ensures that τ_p^+ and $\mathbf{g}^+$ are the same in the two cases. Of course, it is also possible to make these the same by adjusting ρ_p, ρ_f and ν as well, i.e. there are many routes to achieving the same end result.

The route outlined above has the advantage that d^+ is the same for the two cases considered and this may be of some importance when we consider particle interactions with the bottom wall. A similar result may clearly be achieved by keeping $u^*(\mathrm{num}) = u^*(\mathrm{exp})$ but changing ν, d and $\mathbf{g}$. From these considerations, statistics related to particle segregation, ejection frequency and velocity, Lagrangian correlation functions etc., may be scaled for different Reynolds numbers in the wall region. However, for particles outside the wall region (extending say to non-dimensional wall-normal distances of 10–15), scaling with ν is incorrect. The outer scales h and $\bar{u}$ (the mean velocity) become increasingly important. At low Reynolds number is almost proportional to u^*, so u^* can continue to be used as a velocity scale—however, ν must be replaced by h. If we identify

non-dimensional variables scaled with u^* and h by the superscript "$-$", we have the "outer-scaled" analogue of [18] as

$$\frac{d\mathbf{v}^-}{dt^-} = -\frac{\mathbf{v}^- - \mathbf{u}^-}{\tau_p^-} + \mathbf{g}^-. \tag{19}$$

Here we have $\mathbf{v}^- = \mathbf{v}/u^*$ and $\mathbf{u}^- = \mathbf{u}/u^-$, which are the same as $\mathbf{v}^+$ and $\mathbf{u}^+$. However,

$$t^- = \frac{tu^*}{h}; \quad \tau_p^- = \mathrm{Re}\frac{\rho_p}{\rho_f}\frac{d^{-2}}{18}; \quad \mathbf{g}^- = \frac{(\rho_p - \rho_f)hg}{\rho_p u^{*2}},$$

where

$$d^- = \frac{d}{h}.$$

Note that, in comparison to [18],

$$t^+ = \mathrm{Re}\cdot t^-; \quad \mathbf{v}^- = \mathbf{v}^+; \quad \mathbf{u}^- = \mathbf{u}^+ \tag{20a}$$

and

$$\rho_p^+ = \mathrm{Re}\cdot\tau_p^-; \quad \mathbf{g}^+ = \frac{\mathbf{g}^-}{\mathrm{Re}}. \tag{20b}$$

Note that similar particle behaviour is obtained in the outer region by keeping τ_p^- and $\mathbf{g}^-$ the same for different Re in [19]. However, [206] clarifies that it is impossible to do this and keep τ_p^+ and $\mathbf{g}^+$ the same at different Re. We can either keep τ_p^- and $\mathbf{g}^-$ the same or τ_p^+ and $\mathbf{g}^+$ the same at different Re, but not both.

These simple considerations are useful in understanding why particle behaviour in a horizontal channel will depend on two sets of scales (with a transition region in between). This is physically reasonable since particles are periodically ejected from the wall region with velocities proportional to u^*, but the amount of time they spend in the outer flow before falling back depends on h. While in the outer flow they are accelerated towards the local streamwise fluid velocity, since the streamwise velocity in the wall region is much lower. It is clear that how closely they approach the outer streamwise fluid velocity depends on how long particles spend in the outer flow as well as their time constant τ_p.

Before moving on to the actual calculations, it is worth mentioning how boundary–particle interactions are treated in the simulations.

Consider the velocity of a particle to be superscripted with "^" after interaction with a boundary. The conditions applied are

$$(\hat{\mathbf{v}})\cdot\mathbf{n} = -\epsilon\cdot\mathbf{v}\cdot\mathbf{n} \tag{21a}$$

and

$$(\hat{\mathbf{v}})\cdot T = \mathbf{v}\cdot\mathbf{T} - \eta(1+\epsilon)\mathbf{v}\cdot\mathbf{n}. \tag{21b}$$

Here $\mathbf{n}$ is the unit vector normal to the boundary and $\mathbf{T}$ is the unit vector normal to $\mathbf{n}$ in the direction of particle motion, i.e. it is tangential to the boundary. The coefficient of restitution ϵ, is such that $0 \leqslant \epsilon \leqslant 1$ with:

$\epsilon = 1$ for a perfectly elastic collision

and

$\epsilon = 0$ for an inelastic collision.

The coefficient of solid friction, η is such that for $\eta = 0$, the collision is frictionless.

For the calculations reported here, $\eta = 0$ and $\epsilon = 0$, i.e. the particle–wall collisions are inelastic, but frictionless, allowing the particles to move tangentially to the surface without impedance.

The following sections deal with the main results of the simulations based on the discussions above.

3. PARTICLE DISTRIBUTION IN THE WALL REGION

3.1. Method of calculation

The velocity field in an open horizontal channel was obtained using the computational method discussed in the previous section.

The full time-dependent Navier–Stokes equations for the fluid were integrated by the code starting from laminar initial conditions. After statistically steady solutions were attained, the integration continued for some thousand time steps to allow storage of a time series of velocity fields; 64 and 65 modes were used in the spanwise and cross-stream directions and 32 in the streamwise direction, to give reasonably good resolution of the flow field as discussed earlier.

Particles were tracked through the flow, assuming them to be pointwise and subjected to various forces (see [14]). The drag force was always considered. In most cases also a gravity force, directed towards the wall, was introduced. This force was necessary for the simulation of the experiments, as discussed later.

The added mass force was considered for most of the cases reported in table 1, due to the particles and the fluid densities being of the same order of magnitude. Nevertheless, the effect of this force on the particle trajectories was found to be negligible because the particle acceleration relative to the fluid is always small compared to the particle relative velocity. The only exception is the initial transient, where the relative velocity between the particles and the fluid was set to zero.

The fluid velocity at the particle location, appearing in the drag force, was calculated directly through a triple summation of the spectral coefficients (see [13]). This approach assured a high level of accuracy.

The physical parameters for the particles were selected to try to simulate the actual conditions achieved during the experiments of Rashidi *et al.* (1990). All the calculation parameters are summarized in table 1. Of particular interest is the time constant of the particles, which has been previously defined following [18]. If not otherwise specified, the time constant will in subsequent sections refer to the non-dimensional value in wall units (i.e. τ_p^+).

A preliminary analysis showed that the effect of the friction coefficient on the average particle velocity is more significant than that of the restitution coefficient and that both of them are restricted to a region near the wall whose depth is slightly higher than the particles diameter: for this reason ϵ and η were set to zero in the wall boundary condition for the particles given in [21].

At the beginning of the calculation the particles were given a uniform random distribution on a plane located in the wall region. Essentially the particles were pointwise, but allowed to approach the wall only up to a minimum distance given by their radius.

3.2. Results

As discussed in the introduction, the flow near the wall is characterized by streaks of fluid moving at different velocities. Our calculations showed that the interaction between these turbulence structures and the particle distribution near the wall is strongly dependent on the particle time constant. In figure 1 the particle position after 1800 time steps from the start of the calculation is superimposed on the fluid velocity distribution in the wall region for two different particle time constants. Only particles between the wall and $z^+ = 14$ are included in the photographs. It is very clear that particles with a large time constant ("heavy" or "big" particles) tend to segregate in the low-speed streaks, while the "light" particles keep a more uniform distribution, showing a

Table 1. Synopsis of the performed calculation

Case	No. of particles	No. of time steps	Starting z^+	d (mm)	d^+	τ_p^+	ρ_p	Forces: Gravity g^+	Forces: Added mass
1	2000	1800	20	1.1	11.8	8	1.03	0.33	Yes
2	2000	1800	17.9	0.65	6.97	2.78	1.03	0.33	Yes
3	2000	3000	16.6	0.39	4.18	1	1.03	0.33	Yes
4	2000	3000	15.8	0.22	2.36	0.32	1.03	0.33	Yes
5	2000	3000	15.3	0.12	1.29	0.1	1.03	0.33	Yes
6	5000	2400	17.9	0.65	6.97	2.78	1.03	0.0	No
7	2000	3000	15.3	0.12	1.29	0.1	1.03	0.0	No

behaviour similar to what is expected for fluid particles. This behaviour becomes stationary shortly after the start of the calculation.

A quantitative estimate of the degree of accumulation of the particles in the low-speed streaks, as a function of their time constant, is given in figure 2. As a measure of particle segregation, we took the ratio between the streamwise component of the fluid velocity at particle locations (ensemble and time averaged) and the fluid streamwise velocity averaged on the whole plane at the same distance from the wall. Only particles whose centre lay between the wall and $z^+ = 14.75$ were considered. The degree of segregation of the particles, which is proportional to the inverse of the above-defined ratio, increases as their time constant increases up to a maximum value, depending on the characteristic time of the turbulence.

In figure 3 the particle distribution in the wall region is plotted vs the difference between the fluid streamwise velocity at the location and the average fluid streamwise component, normalized by the latter velocity. The maximum concentration of particles is in those regions with a fluid velocity ranging between 1/3 and 2/3 of the averaged fluid velocity. The narrowest distribution is for $\tau_p^+ = 2.78$.

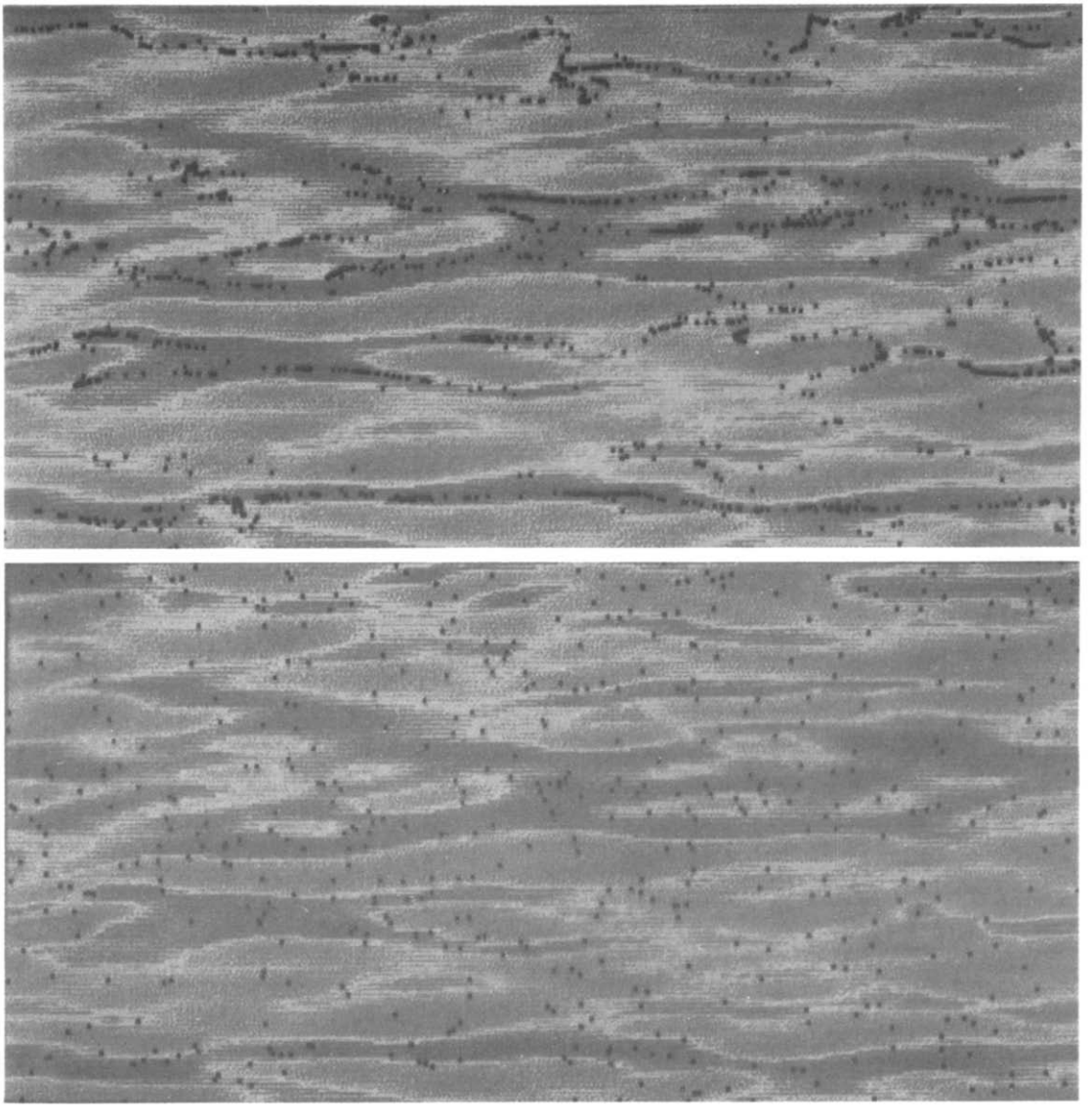

Figure 1. Particle distribution near the wall for different particle time constants. The darker areas are high-speed flow regions, the lighter areas are low-speed flow regions.

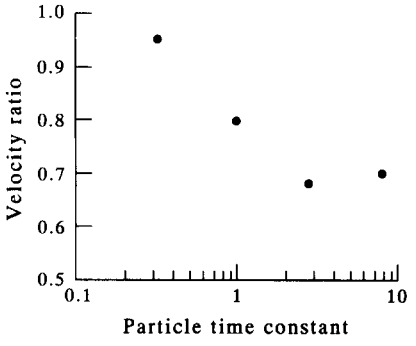

Figure 2. Ratio between the fluid velocity at the particle location and the average fluid velocity.

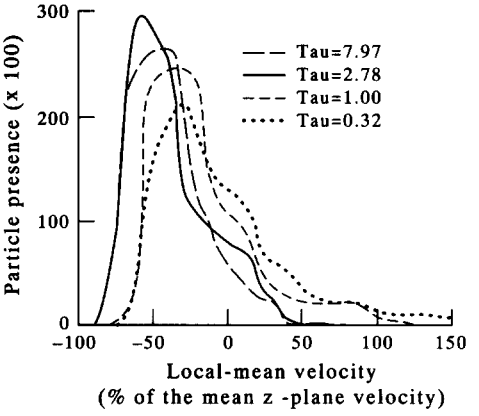

Figure 3. Particles segregation in the low-speed regions. Intermediate time constant (2.78) particles show enhanced segregation.

The different behaviour of the particles, as a function of their time constant, can be explained by considering the time constant of the turbulence structures. We observed that in our calculations the Eulerian time constant of the turbulence structures is higher than the time constants of the particles considered. Therefore, if there is a mechanism that segregates particles inside the low-speed streaks, they will remain trapped if their time constant is small enough to allow them to follow the streak motion, but not so small as to be sensitive to the high-frequency fluctuations, which could redistribute the particles uniformly. This segregation mechanism can be due to the presence of a rotation motion in the high-speed regions which pushes the particles out of them. The presence of gravity has probably an enhancing effect on this mechanism, in the sense that the particles pushed away from the high-speed regions do not go into the bulk flow, but remain in the wall region and finally are trapped in a low-speed streak. The streamwise rotational motion of fluid structures that influence particle trajectories is discussed in a later section.

4. PARTICLE AND FLUID VELOCITIES

4.1. Comparisons between calculations and experiments

The results of the calculations were used also for a comparison with the experiments of Rashidi *et al.* (1990), who published some measurements of particle velocity and concentration in a turbulent water flow through an horizontal channel. These results should have been obtained for $Re = 5000$, corresponding to $Re = 147$ to be consistent with the Rashidi *et al.* experiments. Since this value is too high for our present computational possibilities, a scaling was introduced to simulate the experiments with a flow characterized by a lower Reynolds number, as discussed earlier using [18], i.e. the scaling used wall units to correct for the differences in Reynold's numbers in the section following [18]. Note, however, that this type of scaling has limitations, as discussed earlier, since it breaks down except near the wall.

In our simulation we could obtain a significant number of particles rising from the wall towards the free surface of the channel only for small time constant particles. In this case, their concentration is given in figure 4. In figure 5 the relative velocity between the fluid and the particles is shown for two different values of the particles' time constant. All these data were obtained neglecting the initial phase of the simulation, in order to avoid the effect of the initial distribution and relative velocity, and by introducing a time average of the data up to the end of the calculation. Particles characterized by a larger time constant do not follow the fluid velocity as quickly as lighter particles, as a consequence, the relative velocity is larger for particles at the front.

In figure 6 the experimental data are also shown. The comparison is not completely satisfactory; in fact the calculated relative velocity between the fluid and the particles is significantly lower than the measured one.

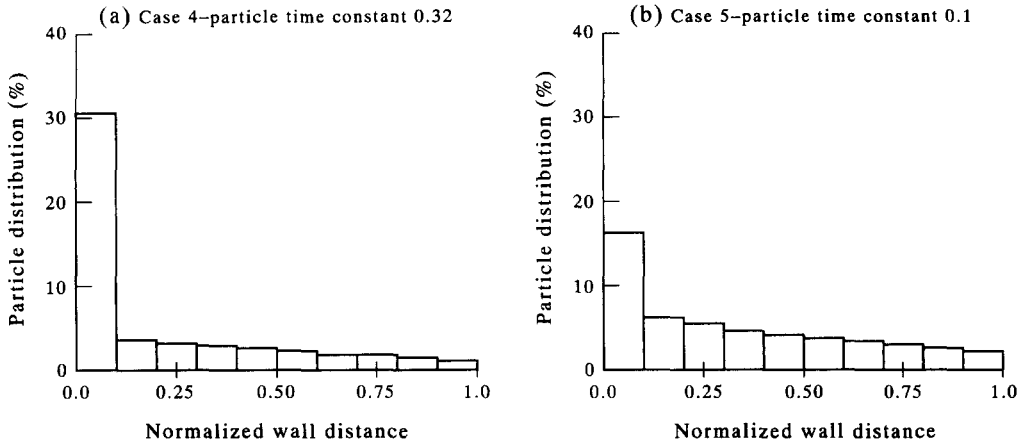

Figure 4. Particle distribution rates as a function of the non-dimensional distance from the wall for different particle time constants.

To give an explanation for this discrepancy we have to consider that the particle distribution is the result of two opposing mechanisms: the first is particle lifting, due the the fluid bursts; the second is particle settling, due mainly to gravity. Even the relative streamwise velocity between the particles and the fluid is given by a balance of two opposite effects. In fact, rising particles usually have a lower velocity than the fluid, while falling particles have a higher one. As discussed before, the scaling adopted is not correct far from the wall; it leads to too long a residence time of the particles in the upper region of the channel, allowing them to be accelerated closer to the fluid velocity by the drag. Thus, we could not account for the diffeence in the experimental and numerical Reynolds numbers by scaling with wall variables. However, the qualitative features leading to the velocity difference were clarified even though there were quantitative differences.

Part of the discrepancy could also be due to the large uncertainty existing in the experiments about the particle density, which has a strong effect on the ratio between the drag and gravity forces.

4.2. *Particle trajectories*

In spite of the poor quantitative agreement between the experiments and calculations, some of the basic mechanisms for particle transport through the flow field were clarified by the simulation. In figure 7 a typical trajectory of a particle during the rise and fall is superimposed on the velocity vector field in a cross-stream section. (The vector field, of course, changes while the particle is

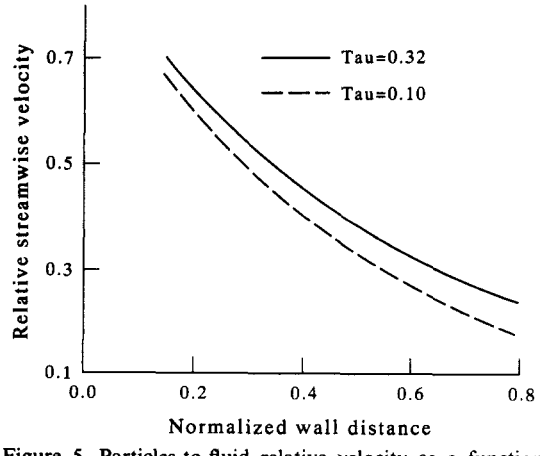

Figure 5. Particles-to-fluid relative velocity as a function of the wall distance for different particle time constants.

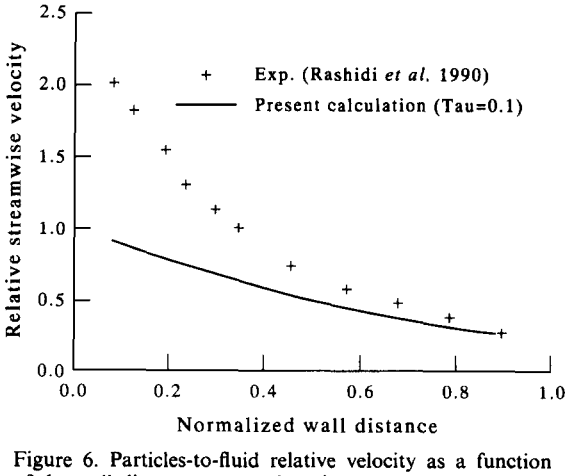

Figure 6. Particles-to-fluid relative velocity as a function of the wall distance: comparison between calculations and experiments.

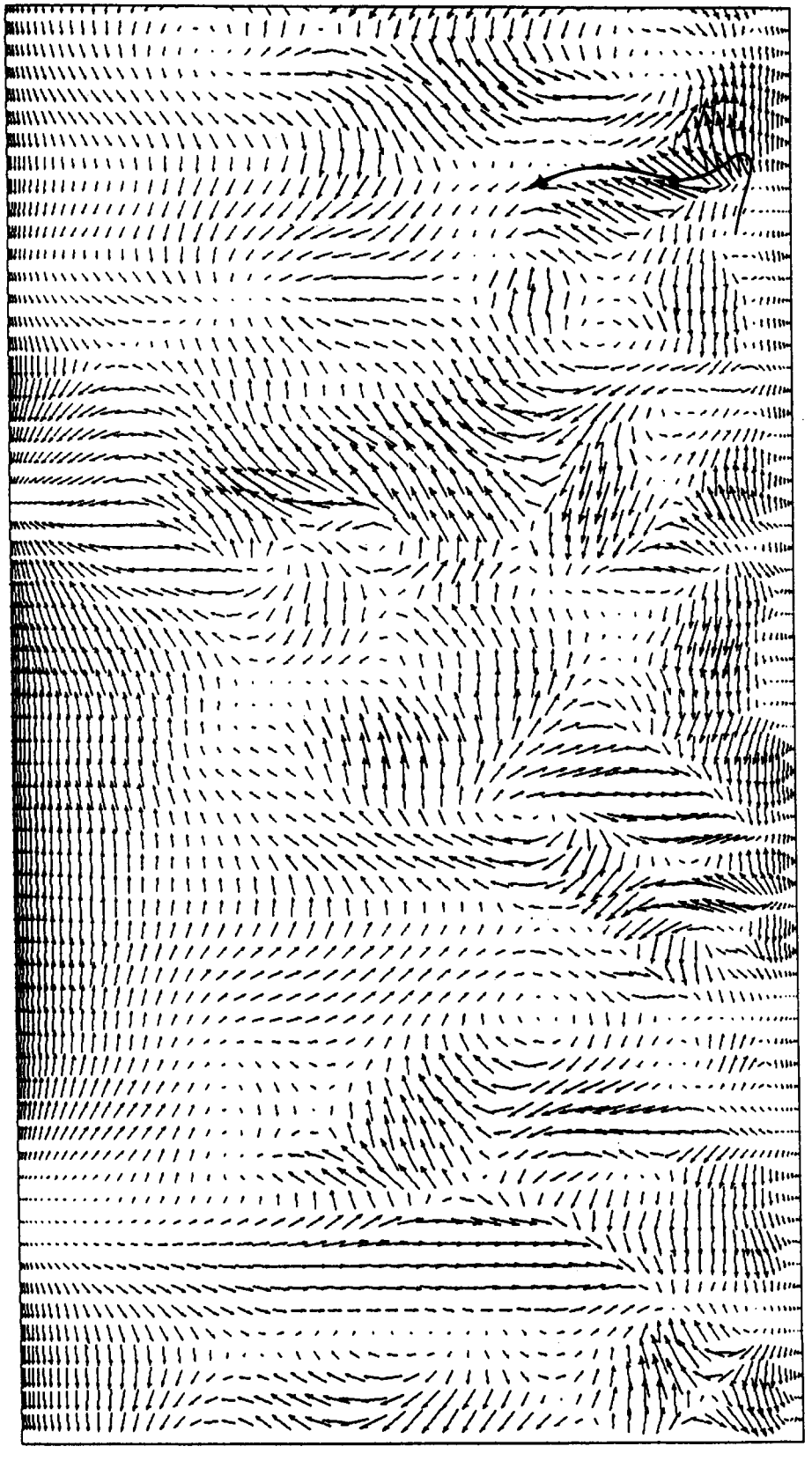

Figure 7. Trajectory of a particle entrained by a turbulent structure. The cross-stream section of the low velocity is taken at the time that corresponds to the spot on the particle trajectory.

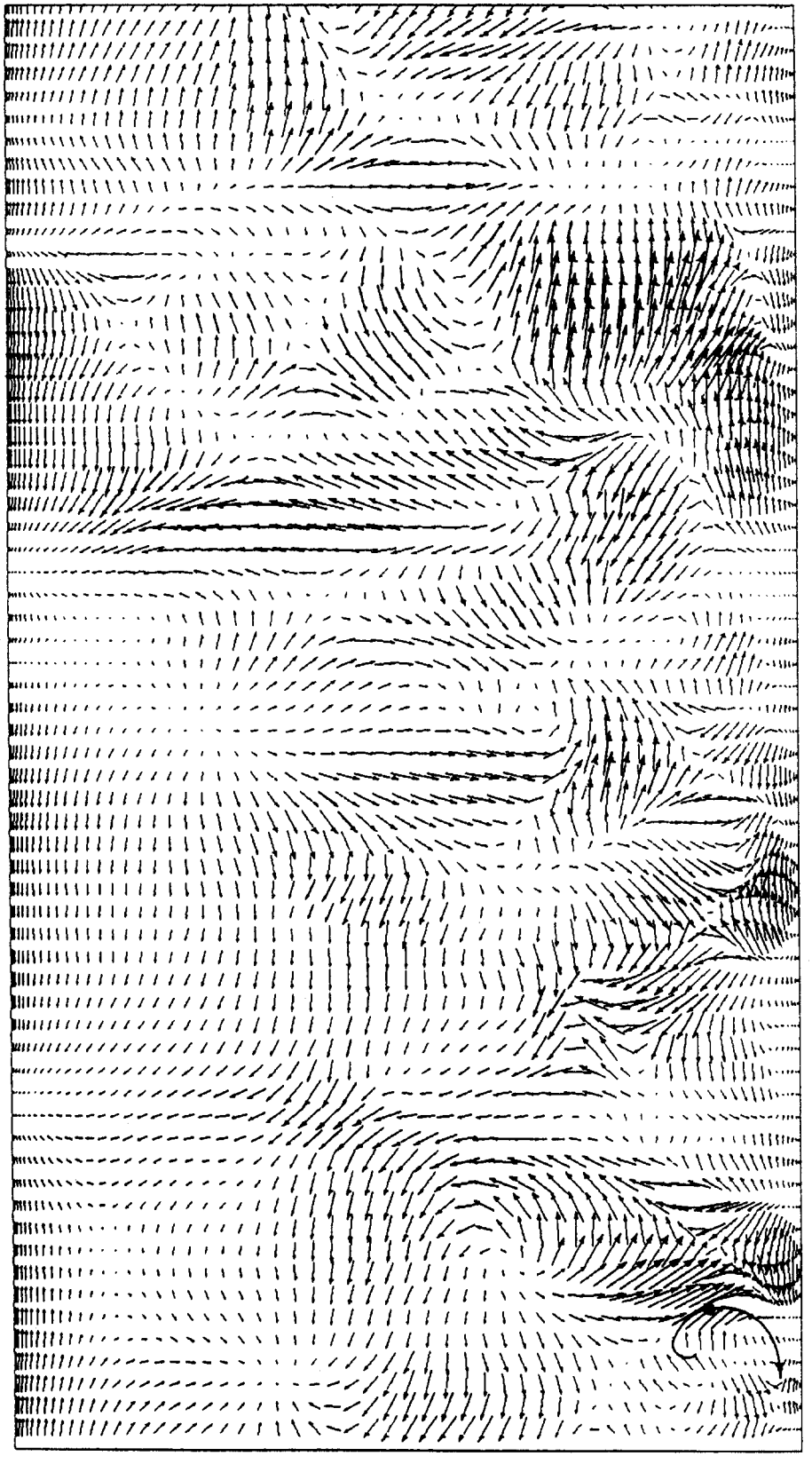

Figure 8. Trajectory of a particle pushed to the wall by an emission of high-momentum fluid. The cross-stream section of the flow velocity is taken at the time that corresponds to the spot on the trajectory.

moving, but the turbulence structures acting on the particle are the same for some time.) It is quite clear how the particle rises due to an upflow caused by one (or two) quasi-streamwise vortices which detach a low-speed mass of fluid from the wall. While the mass of fluid is continuing its movement towards the free surface, the particle goes back to the wall due to gravity. Figure 8 shows a particle trapped in an inrush of high-momentum fluid into the wall region. The figure also illustrates the vortical motion in the cross-stream plane, which probably causes particle segregation into low-speed regions.

5. EFFECTS OF GRAVITY

5.1. Simulations in the absence of gravity

In order to explore the influence of gravity on particle segregation and velocity, two more cases were run. The cases were characterized by particles with the same time constants as the experiments: the first one is the time constant that gives the most segregation; the second is the smallest characteristic time.

5.2. Particle segregation

Figure 9 shows the particles' positions superimposed on the fluid field for the particle time constant that gave the most segregation in presence of gravity. As we can see in comparison with figure 1(a), gravity enhances particle segregation: this result can be explained by thinking of particle motion as a balance between two different effects. The first effect is segregation, probably due to particles being flung out of the quasi-streamwise vortices that deposit them on the wall, see figure 8 for a typical trajectory. The second effect is resuspension of the particle due to an ejection, also caused by quasi-streamwise vortices that cause an upflow, as in figure 7. However, in the presence of gravity the ejections have to be more forcible to resuspend particles. Therefore, more particles stay near the wall and have a chance to segregate. In the absence of gravity the ejections tend to redistribute particles out of the low-speed streaks more easily. Hence more particles are found in the bulk flow, and are distributed more uniformly.

5.3. Particles and fluid velocities

In the absence of gravity particles are pushed to the wall only by the drag force, associated with quasi-streamwise vortices that cause insweeps, so, in figure 10, they appear uniformly distributed.

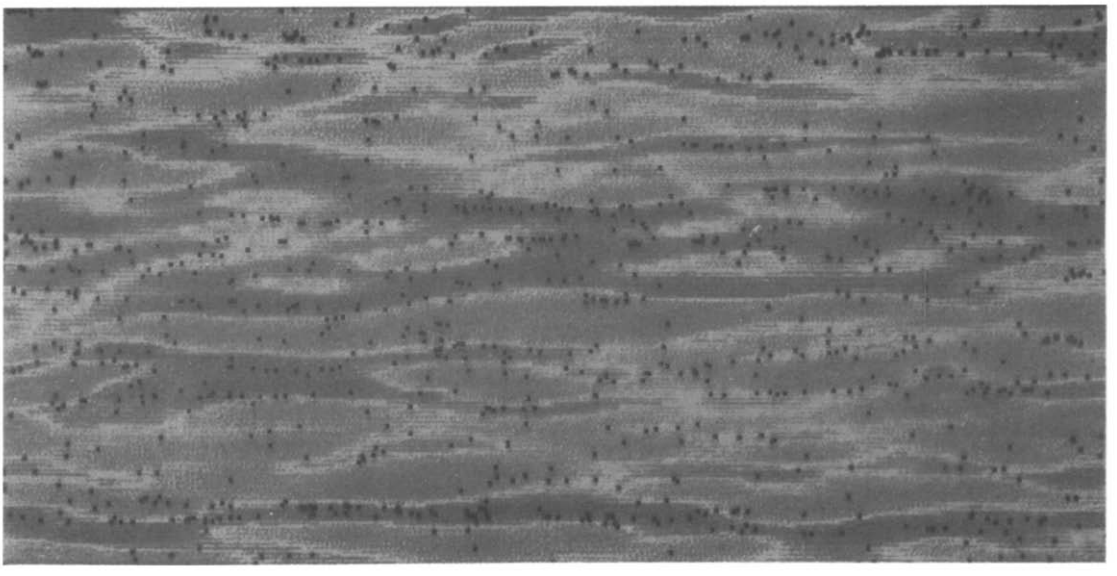

Figure 9. Particle distribution near the wall in the absence of gravity. The darker areas are high-speed flow regions, the lighter areas are low-speed flow regions.

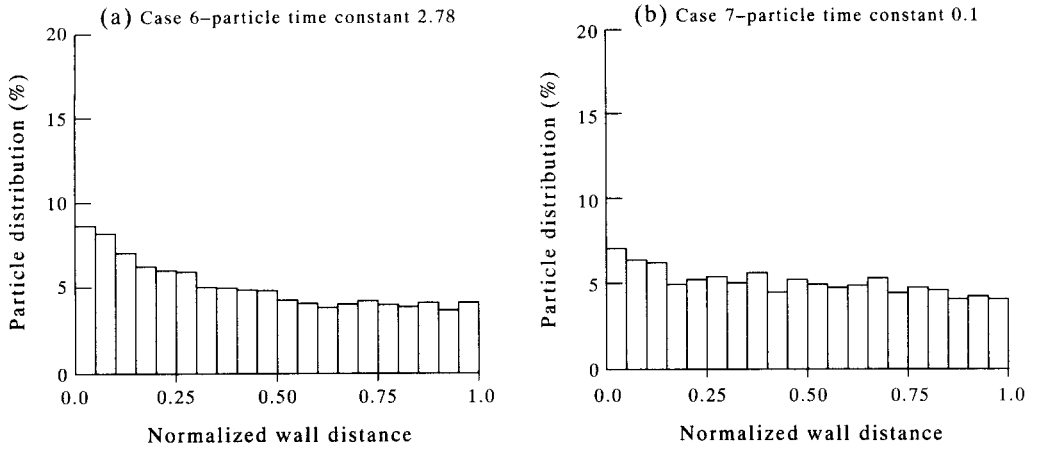

Figure 10. Particle distribution rates vs the non-dimensional distance from the wall for different particle time constants in the absence of gravity.

In figure 11, the relative velocities between the fluid and particles, for the cases with and without gravity, are compared. The particle time constant corresponds to the smallest one used in the Rashidi *et al.* (1990) experiments.

The lag of particles is larger in the absence of gravity, mainly in the neighbourhood of the wall, where the gradient of the fluid streamwise velocity is a maximum. This may be due to more particles from the wall region being resuspended. The effect is not yet completely clear and more numerical experiments are necessary, but a quantitative explanation is as follows.

As seen previously, falling particles contribute to a decrease in the relative velocity while segregated particles ejected from the wall tend to increase it, so the simulation result may be caused by two opposite effects. The number of falling particles is less in the absence of than in the presence of gravity: this contributes to an increase in the relative velocity. However, the number of particles segregated to low-speed regions near the wall is less in the absence of than in the presence of gravity: this contributes to a decrease in the relative velocity but is a secondary effect compared to the previous one, since it is mainly the low-speed regions that are ejected and with them the associated particles.

6. CONCLUSIONS

The simulations indicate that particle segregation depend on the time constant, non-dimensionalized with inner variables when we consider the wall region. For non-dimensional time constants

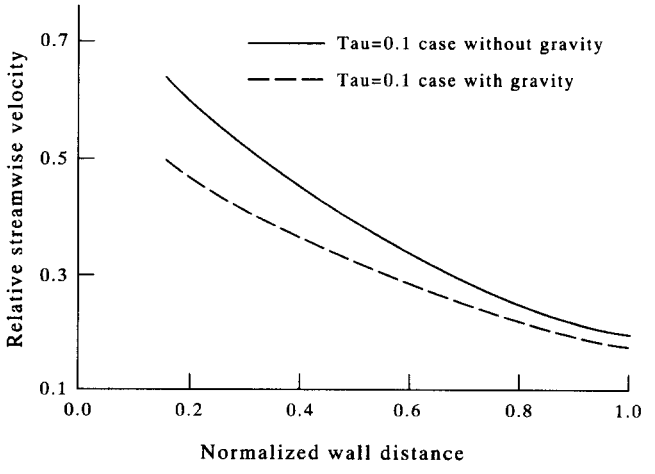

Figure 11. Particles-to-fluid relative velocity as a function of the wall distance: comparison between calculations with and without gravity.

of about 3, the segregation tendency is a maximum. Furthermore, the numerical simulations indicate that particles are ejected from the wall due to upflow caused by quasi-streamwise vortices. However, due to gravity, they fall back to the wall faster than the fluid which is simultaneously ejected. In addition to gravity, the particles are often caught in insweep regions caused by the quasi-streamwise vortices.

While the simulations are in qualitative agreement with the experiments so far as the particle distribution in the wall-normal direction and the particle fluid velocity difference is concerned, there are quantitative differences. The reason for this appears to arise from the two different scales associated with particle motion, i.e. the inner and outer scales. Thus, we are unable to scale the Reynolds number for the two. At present, the higher Reynolds numbers in the experiment could not be simulated numerically, so quantitative comparisons were not possible. Nonetheless, the numerical simulations indicate important effects, such as the effect of the particle time constant on segregation, which deserve further experimental investigation.

Acknowledgements—The authors wish to thank A. Soldati (Department of Chemical Engineering, University of Pisa), for useful discussions in evaluating the results of the calculations, and M. Gremigni (ENEL—Thermal and Nuclear Research Center, Pisa), for support in data visualization.

REFERENCES

CANUTO, C., HUSSAINI, M. Y., QUARTERONI, A. & ZANG, T. A. 1988 *Spectral Methods in Fluid Dynamics*. Springer-Verlag, New York.

CHEIN, R. & CHUNG, J. N. 1987 Effect of vortex pairing on particle dispersion in turbulent shear flows. *Int. J. Multiphase Flow* **13,** 785–802.

GOTTLIEB, D. & ORZAG, S. 1977 *Numerical Analysis of Spectral Methods: Theory and Applications*. SIAM, Philadelphia, PA.

KAMULU, N., TANG, L., TROUTT, T. R., CHUNG, J. N. & CROWE, C. T. 1989 In *Proc. Int. Conf. on Mechanics of Two Phase Flows*, Taipei, Taiwan, pp. 199–202.

KIM, J., MOIN, P. & MOSER, R. 1987 Turbulence statistics in fully developed channel flow at low Reynolds number. *J. Fluid Mech.* **177,** 133–166.

KOBAYASHI, H., MASUTANI, S. M., AZUHATA, S., ARASHI, N. & HISHINUMA, Y. 1988 In *Transport Phenomena in Turbulent Flows* (Edited by HIRATA, M. & KASAGI, N.), pp. 433–466. Hemisphere, New York.

LAM, K. L. 1989 Numerical investigation of turbulent flow by a wall and a free-slip surface. Ph.D. Thesis, Univ. of California, Santa Barbara, CA.

LAM, K. L. & BANERJEE, S. 1988 Investigation of turbulent flow bounded by a wall and a free surface. In *Fundamentals of Gas–Liquid Flows* (Edited by MICHAELIDES, E. E. & SHARMA, M. P.), Vol. 72, pp. 29–38. ASME, Washington, DC.

LAM, K. & BANERJEE, S. 1992 On the condition for streak formation in bounded flow. *Phys. Fluids* **A4,** 306–320.

LANCZOS, C. 1956 *Applied Analysis*. Prentice-Hall, Englewood Cliffs, NJ.

LAZARO, B. J. & LASHERAS, J. C. 1989 Particle dispersion in a turbulent plane free shear layer. *Phys. Fluids* **A1,** 1035–1044.

MAXEY, M. R. 1987 The gravitational settling of aerosol particles in homogeneous turbulence and random flow fields. *J. Fluid Mech.* **174,** 441–465.

MCLAUGHLIN, J. B. 1989 Aerosol particle deposition in numerically simulated channel flow. *Phys. Fluids* **A1,** 1211–1224.

RASHIDI, M., HETSRONI, G. & BANERJEE, S. 1990 Particle–turbulence interaction in a boundary layer. *Int. J. Multiphase Flow* **16,** 935–949.

SCHNACK, D. D., BAXTER, D. C. & CARAMANA, E. J. 1984 A pseudospectral algorithm for three-dimensional magnetohydrodynamic simulation. *J. Comput. Phys.* **55,** 485–514F.

SQUIRES, K. D. & EATON, J. K. 1990 Particle response and turbulence modification in isotropic turbulence. *Phys. Fluids* **A2,** 1191–1203.